1   *Title*

2   **Type 2 and interferon inflammation strongly regulate SARS-CoV-2 related gene**

3   **expression in the airway epithelium**

4

5

6   *Authors/Affiliations*

7   Satria P. Sajuthi[1#], Peter DeFord[1#], Nathan D. Jackson[1], Michael T. Montgomery[1],

8   Jamie L. Everman[1], Cydney L. Rios[1], Elmar Pruesse[1], James D. Nolin[1], Elizabeth G.

9   Plender[1], Michael E. Wechsler[2], Angel CY Mak[3], Celeste Eng[3], Sandra Salazar[3], Vivian

10   Medina[4], Eric M. Wohlford[3,5], Scott Huntsman[3], Deborah A. Nickerson[6,7,8], Soren

11   Germer[9], Michael C. Zody[9], Gonçalo Abecasis[10], Hyun Min Kang[10], Kenneth M. Rice[11],

12   Rajesh Kumar[12], Sam Oh[3], Jose Rodriguez-Santana[4], Esteban G. Burchard[3,13], Max A.

13   Seibold[1,14,15]*

14

15   [1]Center for Genes, Environment, and Health, National Jewish Health, Denver, CO,

16   80206 USA; [2]Department of Medicine, [14]Department of Pediatrics, National Jewish

17   Health, Denver, CO, 80206 USA; [15]Division of Pulmonary Sciences and Critical Care

18   Medicine, University of Colorado-AMC, Aurora, CO, 80045 USA, [3]Department of

19   Medicine, [5]Division of Pediatric Allergy and Immunology, [13]Department of

20   Bioengineering and Therapeutic Sciences University of California San Francisco, San

21   Francisco, CA; [6]Department of Genome Sciences, University of Washington, Seattle,

22   WA, USA, [7]Northwest Genomics Center, Seattle, WA, USA [8]Brotman Baty Institute,

23   Seattle, WA, USA; [9]New York Genome Center, NYC, New York; [10]Center for Statistical

24   Genetics, University of Michigan, Ann Arbor, MI, USA; [11]Department of Biostatistics,

25   University of Washington, Seattle, WA, USA; [4]Centro de Neumología Pediátrica, San

26   Juan, Puerto Rico; [12]Ann and Robert H. Lurie Children's Hospital of Chicago,

27   Department of Pediatrics, Northwestern University, Chicago, Ill [#]these authors

28   contributed equally to this work, *correspondence: seiboldm@njhealth.org

29

30

31 *Abstract*

32

33 Coronavirus disease 2019 (COVID-19) outcomes vary from asymptomatic infection to

34 death. This disparity may reflect different airway levels of the SARS-CoV-2 receptor,

35 ACE2, and the spike protein activator, TMPRSS2. Here we explore the role of genetics

36 and co-expression networks in regulating these genes in the airway, through the

37 analysis of nasal airway transcriptome data from 695 children. We identify expression

38 quantitative trait loci (eQTL) for both *ACE2* and *TMPRSS2*, that vary in frequency

39 across world populations. Importantly, we find *TMPRSS2* is part of a mucus secretory

40 network, highly upregulated by T2 inflammation through the action of interleukin-13, and

41 that interferon response to respiratory viruses highly upregulates *ACE2* expression.

42 Finally, we define airway responses to coronavirus infections in children, finding that

43 these infections upregulate *IL6* while also stimulating a more pronounced cytotoxic

44 immune response relative to other respiratory viruses. Our results reveal mechanisms

45 likely influencing SARS-CoV-2 infectivity and COVID-19 clinical outcomes.

46

47

48

49

50

51

52

53

3

54   *Introduction*

55

56   In December of 2019, a novel Coronavirus, SARS-CoV-2, emerged in China and has

57   gone on to trigger a global pandemic of Coronavirus Disease 2019 (COVID-19), the

58   respiratory illness caused by this virus[1]. While most individuals with COVID-19

59   experience mild cold symptoms (cough and fever), some develop more severe disease

60   including pneumonia, which often necessitates mechanical ventilation[2]. In fact, an

61   estimated 5.7% of COVID-19 illnesses are fatal[3]. Enhanced risk of poor outcomes for

62   COVID-19 has been associated with a number of factors including advanced age, male

63   sex, and underlying cardiovascular and respiratory conditions[4, 5]. Yet, while the majority

64   of serious COVID-19 illness occurs in adults over 60, children are also thought to be

65   highly susceptible to infection. Moreover, recent data suggest that 38% of COVID-19

66   cases occurring in children are of moderate severity and 5.8% are severe or critical[6],

67   highlighting a need for studying risk factors of illness in this population as well.

68

69   One factor that may underlie variation in clinical outcomes of COVID-19 is the extent of

70   gene expression in the airway of the SARS-CoV-2 entry receptor, *ACE2*, and

71   *TMPRSS2*, the host protease that cleaves the viral spike protein and thus allows for

72   efficient virus-receptor binding[7]. Expression of these genes and their associated

73   programs in the nasal airway epithelium is of particular interest given that the nasal

74   epithelium is the primary site of infection for upper airway respiratory viruses, including

75   coronaviruses, and acts as the gateway through which upper airway infections can

76   spread into the lung. The airway epithelium is composed of multiple resident cell types

77   (e.g., mucus secretory, ciliated, basal stem cells, and rare epithelial cell types)

78   interdigitated with immune cells (e.g. T cells, mast cells, macrophages), and the relative

79   abundance of these cell types in the epithelium can greatly influence the expression of

80   particular genes[8-10], including *ACE2* and *TMPRSS2*. Furthermore, since the airway

81   epithelium acts as a sentinel for the entire respiratory system, its cellular composition,

82   along with its transcriptional and functional characteristics, are significantly shaped by

83   interaction with environmental stimuli. These stimuli may be inhaled (e.g., cigarette

84   smoke, allergens, microorganisms) or endogenous, such as when signaling molecules

85   are produced by airway immune cells present during different disease states. One such

86   disease state is allergic airway inflammation caused by type 2 (T2) cytokines (IL-4, IL-5,

87   IL-13), which is common in both children and adults and has been associated with the

88   development of both asthma and COPD in a subgroup of patients[11-13]. T2 cytokines are

89   known to greatly modify gene expression in the airway epithelium, both through

90   transcriptional changes within cells and epithelial remodeling in the form of mucus

91   metaplasia[11, 14, 15]. Microbial infection is another strong regulator of airway epithelial

92   expression. In particular, respiratory viruses can modulate the expression of thousands

93   of genes within epithelial cells, while also recruiting and activating an assortment of

94   immune cells[16-18]. Even asymptomatic nasal carriage of respiratory viruses, which is

95   especially common in childhood, has been shown to be associated with both genome-

96   wide transcriptional re-programming and infiltration of macrophages and neutrophils in

97   the airway epithelium[19], demonstrating how viral infection can drive pathology even

98   without overt signs of illness.

99

100   Genetic variation is another factor that may regulate gene expression in the airway

101   epithelium. Indeed, expression quantitative trait loci (eQTL) analyses carried out in

102   many tissues have suggested that as many as 70% of genes expressed by a tissue or

103   organ are under genetic control[20]. Severity of human rhinovirus (HRV) respiratory illness

104   has specifically been associated with genetic variation in the epithelial genes *CDHR3*[21]

105   and the *ORMDL3*[22] and, given differences in genetic variation across world populations,

106   it is possible that functional genetic variants in SARS-CoV-2-related genes could partly

107   explain population differences in COVID-19 clinical outcomes.

108

109   Finally, there are important questions regarding the host response to SARS-CoV-2

110   infection. For example, it is unclear whether specific antiviral defenses in the epithelium

111   are blocked by SARS-CoV-2 or whether the virus may trigger epithelial or immune cell

112   pathways that prolong airway infection, and/or even incite a hyperinflammatory state in

113   the lungs in some individuals that leads to more severe disease. Although large cohorts

114   of subjects infected by the novel coronavirus are still lacking, much can be learned by

115   exploring transcriptional responses to other coronavirus strains. In particular, because

116   nasal airway brushings capture both epithelial and immune cells present at the airway

117   surface, such samples collected from a cohort of subjects infected by a range of viruses

118   provide an opportunity to comprehensively investigate the potentially varied and

119   cascading effects of coronavirus infection on airway expression and function.

120

121   In this study, we first use single cell RNA-sequencing (scRNA-seq) to elucidate the

122   cellular distribution of *ACE2* and *TMPRSS2* expression in the nasal airway epithelium.

123   We also perform network and eQTL analysis of bulk gene expression data on nasal

124   airway epithelial brushings collected from a large cohort of asthmatic and healthy

125   children in order to identify the genetic and biological regulatory mechanisms governing

126   *ACE2* and *TMPRSS2* expression. We then use multi-variable modeling to estimate the

127   relative contribution of these factors to population variation in the expression of these

128   two genes, and by performing experiments on mucociliary airway epithelial cultures

129   confirm a dominant role for both T2 inflammation and viral infection in regulating

130   expression of *ACE2* and *TMPRSS2*. Finally, we define the cellular and transcriptional

131   responses to *in vivo* coronavirus infections in the nasal airway of children.

132

133

134

135

136

137

138

139

140

141

142

143

144

145

146   *Results*

147

148   **ACE2 and TMPRSS2 are expressed by multiple nasal airway epithelial cell types**

149

150   We first examined *ACE2* and *TMPRSS2* expression at a cell type level through single

151   cell RNA sequencing (scRNA-seq) of a nasal airway epithelial brushing from an

152   asthmatic subject. Shared Nearest Neighbor (SNN)-based clustering of 8,291 cells

153   identified 9 epithelial and 3 immune cell populations (Figure 1a, Supplementary Table

154   1). We found that 7 epithelial cell populations contained *ACE2*⁺ cells (at low frequency),

155   with the highest frequency of positive cells found among basal/early secretory cells,

156   ciliated cells, and secretory cells (Figure 1b). We did not observe meaningful *ACE2*

157   expression among any of the immune cell populations, which included T cells, dendritic

158   cells, and mast cells. We found *TMPRSS2* to be expressed by all epithelial cell types,

159   with a higher frequency of positive cells among the different cell types, compared to

160   *ACE2* (Figure 1b,c). A small number of mast cells were also *TMPRSS2*⁺ (Figure 1c).

161

162

163   **TMPRSS2 is part of a mucus secretory co-expression network highly induced by**

164   **T2 inflammation**

165

166   We next sought to determine the variation in nasal epithelial expression of *ACE2* and

167   *TMPRSS2* across healthy and asthmatic children, and to identify biological mechanisms

168   that regulate this variation. Thus, we performed weighted gene co-expression network

8

169   analysis (WGCNA) on whole transcriptome sequencing data from nasal airway

170   brushings of 695 Puerto Rican healthy and asthmatic children in the Genes-

171   Environments and Asthma in Latino Americans II study (GALA II). This analysis

172   identified 54 co-expression networks representing cell type-specific expression

173   programs such as ciliogenesis, mucus secretion, and pathways of immunity and airway

174   inflammation (Supplementary Table 2). The *TMPRSS2* gene was contained within one

175   of a set of three highly correlated networks exhibiting strong enrichments for mucus

176   secretory cell genes and pathways (Figure 2a, Supplementary Table 2,3). For example,

177   the black network, which was highly correlated with *TMPRSS2* expression (r=0.64,

178   p=1e-82), was strongly enriched for *Golgi mediated transport* and *COPI-dependent*

179   *Golgi to ER transport* pathways, both of which are involved in the normal processing

180   and transport of mucin proteins (Figure 2a). *TMPRSS2* itself fell within and was highly

181   correlated with expression of the pink network (r=0.68, p=3e-97), which was highly

182   enriched for *mucus goblet cell* markers (p=2e-6, Figure 2a,b). The pink network was

183   also enriched for genes involved in the *O-linked glycosylation of mucins* pathway (p=9e-

184   4), which is vital to the function of mucus secretory cells, especially those induced by T2

185   inflammation (r=0.68, p=3e-97, Figure 2a,b). In fact, we found that this network

186   contained the T2 cytokine *IL13* while being particularly enriched for genes known to

187   mark and transcriptionally regulate IL-13-induced mucus metaplasia (*FCGBP, SPDEF,*

188   *FOXA3*). The saddle brown network was also related to mucus secretory cells, and

189   contained the most canonical T2 inflammation markers[11, 23] including *POSTN*, *CLCA1*,

190   *CPA3*, *IL1RL1*, *CCL26,* and was strongly correlated with both *TMPRSS2* (r=0.61, p=5e-

191   72, Figure 2c) and the other T2 mucus secretory network (pink) (r=0.92, p=3e-280,

192   Supplementary Table 4). In contrast, we found *ACE2* expression to be strongly

193   negatively correlated with expression of both T2 networks (pink: r=-0.61, p=3e-72,

194   saddle brown: r=-0.7, p=2e-102, Figure 2e,f). To identify subjects with high and low T2

195   inflammation, we hierarchically clustered all subjects based on the expression of genes

196   in the canonical T2 network (saddle brown). This resulted in the identification of two

197   distinct groups we labeled as T2-high (n=364) and T2-low (n=331) (Supplementary

198   Figure 1a). We found that this expression-derived T2 status was strongly associated

199   with traits known to be driven by T2 inflammation including IgE levels, exhaled nitric

200   oxide (FeNO), blood eosinophils, and asthma diagnosis (Supplementary Figure 1b-e).

201   Notably, *TMPRSS2* levels were 1.3-fold higher in T2-high subjects (p=1e-62), while,

202   *ACE2* expression was 1.4-fold lower in T2-high subjects (p=2e-48) (Figure 2d,g).

203

204   To investigate whether the strong *in vivo* relationship between airway T2 inflammation

205   and *TMPRSS2*/*ACE2* expression is causal in nature, we performed *in vitro* stimulation

206   of paired air-liquid interface (ALI) mucociliary airway epithelial cultures with 72 hours of

207   IL-13 or mock stimulus (n=5 donors, Figure 3a). Performing paired differential

208   expression analysis between the mock and IL-13 stimulated cultures, we found that

209   *ACE2* and *TMPRSS2* were strongly down- and up-regulated, respectively, supporting

210   our *in vivo* analysis results ($\log_2$FC= -0.67, p=5e-3, $\log_2$FC= 1.20, p=5e-9, Figure 3b,c).

211   To better understand the cellular basis of *TMPRSS2* and *ACE2* regulation by IL-13, we

212   leveraged scRNA-seq data previously generated on tracheal airway epithelial cultures

213   that were chronically stimulated (10 days) with IL-13 or control media (Figure 3a,d).

214   Similar to our results from *in vivo* nasal scRNA-seq data, we observed that *ACE2*

10

215   expression was highest among basal, ciliated, and early/intermediate secretory cell

216   populations, with *ACE2* being significantly downregulated by IL-13 among both basal

217   and intermediate secretory cells (Figure 3e). Also mirroring the *in vivo* scRNA-seq data,

218   *TMPRSS2* was expressed across all epithelial cell types, but at a higher frequency

219   among secretory cells (Figure 3f). IL-13 stimulation induced dramatic upregulation of

220   *TMPRSS2* in early secretory, intermediate secretory, and mature mucus secretory cell

221   populations (Figure 3f). Furthermore, IL-13 stimulated mucus metaplasia that resulted in

222   the development of a novel mucus secretory cell type and an IL-13 inflammatory

223   epithelial cell that both highly expressed *TMPRSS2* (Figure 3f). Together, our *in vivo*

224   and *in vitro* analyses strongly suggest that *TMPRSS2* is part of a mucus secretory cell

225   network that is highly induced by IL-13-mediated T2 inflammation.

226
227

228

229

230   **ACE2 belongs to an interferon response network that is induced by respiratory**

231   **virus infections**

232

233   Returning to the *in vivo* nasal airway epithelial expression networks, we found that

234   *ACE2* expression was highly correlated with expression of two networks (purple and

235   tan) (purple: r=0.74, p=3e-120, tan: r=0.72, p=2e-110, Figure 4a,b). The purple network

236   was highly enriched for genes that mark cytotoxic T cells and antigen-presenting

237   dendritic cells, both of which are particularly abundant in a virally infected epithelium

238   (Figure 4c, Supplementary Table 2), whereas the tan network was strongly enriched for

239   interferon and other epithelial viral response genes (*IFI6*, *IRF7*, *CXCL10*, *CXCL11*)

240   (Figure 4c, Supplementary Table 2). Clustering of subjects based on the interferon

241   response network genes resulted in two groups, one highly (interferon-high=78) and

242   one lowly (interferon-low=617) expressing these interferon response network genes

243   (Supplementary Figure 2). We found that *ACE2* expression was 1.7-fold higher in the

244   interferon-high vs. interferon-low group (Figure 4d). In a previous study, we found that

245   children with nasal gene expression characteristic of the interferon network tended to be

246   infected with a respiratory virus, despite being asymptomatic[19]. To explore the

247   possibility of this relationship in our current dataset, we metagenomically analyzed the

248   RNA-seq data for all subjects to identify those harboring reads for a respiratory virus.

249   This analysis found that 18% of GALA II children were asymptomatically harboring a

250   respiratory virus from one of eight general respiratory virus groups (Figure 4e).

251   Strikingly, we found that 78% of interferon-high subjects were virus carriers compared to

252   only 10% of interferon-low subjects. These results demonstrate how asymptomatic virus

253   carriage nonetheless stimulates an active viral response that includes *ACE2*.

254

255   To directly test the effect of respiratory virus infection on epithelial *ACE2* gene

256   expression we again employed our ALI mucociliary epithelial culture system. Performing

257   mock or human rhinovirus-A16 infection of mature cultures (Day 27, Figure 4f) from 5

258   donors we found 7.7-fold upregulation of *ACE2* gene expression with HRV-A infection

259   (p=1.3e-51, Figure 4g). In contrast, we only observed a trend for down regulation of

260   *TMPRSS2* gene expression among virally infected subjects (Figure 4h). These results

261   confirm the strong regulation of *ACE2* gene expression by viral infection.

12

262

Genetic determinants of *ACE2* and *TMPRSS2* expression in the nasal airway epithelium

265

We next explored the role of genetic regulatory variants in helping to drive epithelial expression of *ACE2* and *TMPRSS2.* To do this, we performed cis-eQTL analysis for these two genes, using nasal gene expression and genome-wide genetic variation data collected from the GALA II study children. We identified 316 and 36 genetic variants significantly associated with expression of *ACE2* and *TMPRSS2*, respectively (Figure 5a,b). Stepwise forward-backward regression analysis of these eQTL variants revealed a single independent eQTL variant (rs181603331) for the *ACE2* gene (6e-23), located ~20kb downstream of the transcription start site (Figure 5a). This rare eQTL variant (allele frequency [AF]=1%) was associated with a large decrease in *ACE2* expression ($\log_2 A_{FC}$=-1.6) (Figure 5c).

Similar analysis of the *TMPRSS2* eQTL variants yielded three independent eQTL variants (rs1475908 AF=20%, rs74659079 AF=4%, and rs2838057 AF=13%, Figure 5b). The eQTL variant rs1475908 was associated with a decrease in *TMPRSS2* expression ($\log_2 A_{FC}$=-0.37, Figure 5d), whereas both the rs74659079 and rs2838057 eQTL variants were associated with increased *TMPRSS2* expression ($\log_2 A_{FC}$=0.38, 0.43, respectively, Supplementary Figure 3).

282

Examining the frequency of these eQTL variants among eight world populations listed in the gnomAD genetic variation database (v2.1.1), we found that the *ACE2* eQTL variant

285   was only present in people of African descent and at a low frequency (AF=0.7%, Figure

286   5e). In contrast, the *TMPRSS2* eQTL variant associated with decreased expression,

287   rs1475908, occurred across all world populations, with the highest allele frequencies

288   among East Asians (AF=38%), Europeans (AF=35%), intermediate frequencies among

289   Africans (AF=26%) and Ashkenazi Jews (AF=23%), and the lowest frequency among

290   Latinos (AF=17%). The two *TMPRSS2* eQTL variants associated with increased

291   expression exhibited much more disparate allele frequencies across world populations.

292   Namely, the allele frequency of rs74659079 is above 1% only among people of African

293   descent (AF=11%) and 4% in the participating Puerto Rican population. Likewise, the

294   rs2838057 eQTL variant, which was associated with increased *TMPRSS2* expression

295   was present at a frequency of 32% in East Asians, 20% in Latinos, and <10% in all

296   other world populations. Together, these results suggest that if *TMPRSS2* levels

297   influence susceptibility to SARS-CoV-2, then genetics may play a significant role in

298   infection risk and that this risk will vary significantly across world populations.

299

300

301   **Multi-variable modeling of airway *ACE2* and *TMPRSS2* gene expression**

302

303   Our analyses indicate that T2 inflammation, interferon/viral response signaling, and

304   genetics are all determinants of *ACE2* and *TMPRSS2* gene expression in the airway

305   epithelium of children. Therefore, we next sought to determine the relative importance of

306   these factors in determining levels of these genes using multi-variable regression

307   analysis. We included asthma status, age, and sex as model covariates since chronic

308   lung disease, increasing age, and male sex have all been associated with increased risk

309   of poor COVID-19 illness outcomes. Modeling *ACE2* expression among GALA II

310   children, we found that T2 and interferon statuses had the strongest effects on *ACE2*

311   expression (p=1.6e-57, p=6.5e-43, respectively), with T2-low and interferon-high

312   individuals exhibiting the highest levels of expression. These two variables

313   independently explained 24% and 17% of the variance in *ACE2* expression (Table 1).

314   While the *ACE2* eQTL variant, rs181603331, was associated with a notable decrease in

315   *ACE2* levels, it only accounted for 1.2% of the variance, reflecting the low frequency of

316   this variant in our population. Increasing age and asthma diagnosis were both

317   associated with small decreases in *ACE2* expression, although both variables

318   accounted for less than 2% of the variance, and sex was not a significant predictor

319   (Table 1).

320

321   Similar modeling of *TMPRSS2* expression found that T2-high status dramatically

322   increased expression, with an effect size 5.4x larger than any other variable, capturing

323   33% of total variation in *TMPRSS2* (Table 1). While statistically significant, the two

324   *TMPRSS2* eQTL variants associated with increased expression exhibited small effect

325   sizes totaling <1% of variance explained. All other predictors were not significant.

326   Collectively, these modeling results confirm that both T2 and interferon inflammation are

327   strong and antagonistic regulators of *ACE2* expression and show that T2 inflammation

328   is the lone dominant driver of airway expression of *TMPRSS2.*

329

330   **Coronavirus Infections drive an enhanced cytotoxic immune response**

15

331

332   Our metagenomic analysis of RNA-seq data from the nasal brushings identified 18

333   children with viral sequence reads from one of four different coronavirus (CoV) species

334   (OC43, JKU1, 229E, NL63) (Supplementary Table 5). This allowed us to explore airway

335   transcriptomic responses to infection with coronavirus subfamily viruses specifically,

336   which will likely most resemble responses to SARS-CoV-2. To increase the likelihood

337   that these subjects were experiencing an active viral infection, we limited our analysis to

338   the 11 most highly infected subjects, comparing them to all subjects not infected with a

339   virus (n=571). To allow us to discriminate CoV-enhanced responses from those that are

340   more general to respiratory viruses, we also established a virus control group composed

341   of the 37 subjects highly infected with human rhinovirus species (HRV) (Supplementary

342   Table 6). We first compared expression of genes in the cytotoxic immune response

343   (purple) network and interferon response (tan) network (discussed earlier; see Figure

344   4a, b) among these virus infected groups, and found that both networks were more

345   highly expressed in virus-infected individuals (Figure 6a, b). Moreover, while the

346   induction in interferon response was similar for both CoV and HRV groups, induction in

347   the cytotoxic immune response was considerably higher in CoV-infected ($\Delta E_g = 0.049$)

348   compared to HRV-infected individuals ($\Delta E_g = 0.032$, Figure 6b).

349   To further explore this increase in cytotoxic immune response and other potential

350   pathways in CoV-infected individuals, we next performed a transcriptome-wide screen

351   for genes differentially expressed in CoV or HRV-infected groups compared to

352   uninfected individuals. These analyses revealed 2,515 differentially expressed genes

353   (DEGs) with CoV infection and 2,357 DEGs with HRV infection (FDR < 0.05 and $\log_2$FC

16

354   > |0.5|), of which 35% and 31% were only observed with CoV and HRV infections,

355   respectively, based on our significance cutoff (Figure 6c). Upstream regulator analysis

356   with IPA carried out separately on CoV and HRV infection response genes showed that

357   the top cytokines and transcription factors that may regulate these infections are shared

358   between the two virus families, including IL10, IL1B, IFNG, IFNA2, and STAT1 (Figure

359   6d). One inferred upstream regulator of CoV response genes, IL-6, which was also

360   among the genes upregulated with CoV infection (log$_2$FC=2.2, Figure 6e), is especially

361   noteworthy considering that an IL-6 blocking antibody therapy is currently under

362   investigation for use in treatment of COVID-19 illnesses[24]. Additionally, we found *ACE2*

363   among the shared upregulated genes, reinforcing its upregulation in the course of

364   different respiratory virus infections (log$_2$FC in CoV$^+$=0.6, log$_2$FC in HRV$^+$=0.5, Figure

365   6e).

366

367   In trying to understand the biological basis of the viral responses we found to be CoV-

368   specific in our differential expression analysis, we considered whether the differential

369   presence and/or response of various immune cell types was an explanatory factor. To

370   investigate this, we used gene set enrichment analysis (GSEA) to test for enrichment of

371   CoV-specific, HRV-specific, and CoV/HRV-shared DEG sets among gene markers for

372   11 different flow-sorted human immune cell types defined based on whole transcriptome

373   data (citation) (Supplementary Table 7). The shared viral DEGs showed significant

374   enrichment for genes characteristic of macrophages, monocytes, neutrophils, dendritic

375   cells, and NK cells. In contrast, the set of CoV-enhanced DEGs resulted in strong

376   enrichments for both CD8+ T cells and dendritic cells, suggesting an especially

17

377   important role for activation of cytotoxic T cells though antigen presentation by dendritic

378   cells in CoV infections (Figure 6f). Also supporting an enriched cytotoxic response

379   among CoV-infected subjects was a strong enrichment for CoV-specific DEGs among

380   NK cells, which participate heavily in the killing of virally infected cells (Figure 6g). We

381   note that these enrichments were not observed among HRV-enhanced DEGs, which

382   were instead most strongly enriched among neutrophils, as well as eosinophils,

383   macrophages, and monocytes. Furthermore, through pathway analysis we identified

384   multiple pathways related to cytotoxic T cell and NK cell activity that were enriched

385   either specifically or more dramatically among CoV DEGs compared to HRV DEGs

386   (Figure 6e). These results suggest that while CoV infections are highly similar to HRV

387   infections, they likely elicit an enhanced cytotoxic immune response.

388

389   *Discussion*

390

391   Although the high variability in clinical outcomes of COVID-19 illness is now well

392   documented and multiple demographic and clinical traits have been associated with

393   severe disease, little is known about the host biologic factors underlying this variability.

394   In the current study, we reasoned that population variation in upper airway expression

395   of the ACE2 receptor for SARS-CoV-2 and the virus-activating TMPRSS2 protease,

396   would drive infection susceptibility and disease severity. We therefore deployed network

397   and eQTL analysis of nasal airway epithelial transcriptome data from a large cohort of

398   healthy and asthmatic children to determine mechanisms associated with airway

399   expression of these genes, and their relative power in explaining variation in the

400   expression of these genes among children. We observed only weak associations with

401   asthma status, age, and gender among children aged 8-21 years. Moreover, although

402   we found that genetics does influence expression of these genes, the effect of this

403   variation was small in comparison to the dramatic influence of T2 cytokine-driven

404   inflammation on both *ACE2* (downregulation) and *TMPRSS2* (upregulation) expression

405   levels. We found an equally important role for viral-driven interferon inflammation in

406   regulating levels of *ACE2* in the airway. Additionally, through study of *in vivo* upper

407   airway CoV subfamily infections, we not only identify inflammatory regulators of these

408   infections, but also provide evidence that this subfamily of viruses drives an enhanced

409   cytotoxic immune response. Our work provides a set of biomarkers that can be easily

410   examined in COVID-19 patients, through analysis of nasal swabs, to determine the

411   relative importance of these mechanisms and genes in governing susceptibility to

412   infection, severe illness and death.

413

414   Our single cell analysis of an *in vivo* nasal brushing observed *ACE2* expression, albeit

415   at low frequency, primarily among basal, ciliated, and less mature, early secretory cells.

416   These results are supported by a recent report of *ACE2* expression in transient

417   secretory cells, likely a close equivalent to our early secretory population[25]. Although a

418   much higher portion of cells, representing all epithelial cell types, expressed *TMPRSS2*,

419   the low frequency of *ACE2*^{+} cells resulted in very few dual *ACE2*/*TMPRSS2* expressing

420   cells. However, we caution that a cell may not need to be *TMPRSS2*^{+} to be susceptible

421   to infection, since it has been demonstrated the TMPRSS2 protein is secreted from

422   nasal airway epithelial cells[26]. We also caution that scRNA-seq data are known to

423 exhibit biases in gene detection, and thus the level and frequency of *ACE2* expression

424 across cells may be much higher than we observe here. In line with this possibility we

425 observe more moderate levels of *ACE2* expression in our bulk RNA-seq data on nasal

426 brushings.

427

428 Airway inflammation caused by type 2 cytokine production from infiltrating immune cells

429 plays a prominent role in the control of cellular composition, expression, and thus

430 biology of the airway epithelium[11, 13, 23, 27]. Moreover, while T2 airway inflammation is an

431 important driver of T2-high asthma and COPD disease endotypes, it is also associated

432 with atopy in the absence of lung disease, a very common phenotype in both children

433 and adults. In fact, among the children in this study, we find that 43% of non-asthmatics

434 were scored as T2-high based on expression profile, further substantiating the high

435 prevalence of T2 airway inflammation outside of those with lung disease. Our data

436 suggest that airway epithelial *TMPRSS2* expression is highly upregulated by T2

437 inflammation, and specifically by IL-13. Both our network and single cell data show that

438 *TMPRSS2* is most prominent in less developed "early secretory" cells as well as in more

439 mature mucus secretory cells. Based on our *in vitro* data, IL-13 upregulates *TMPRSS2*

440 across nearly all types of epithelial cells, but the core of this effect appears to be in the

441 metaplastic mucus secretory cells that are generated as a consequence of IL-13

442 signaling[14, 15]. In fact, our network data suggest that, although *TMPRSS2* expression is

443 highly correlated with that of a co-expressed network of mucus secretory genes

444 characterizing "normal", non-metaplastic, mucus secretory cells, it's correlated even

445 more strongly with a network that characterizes mucus secretory cells undergoing IL-13-

20

446   induced metaplasia. In contrast to enhanced levels of *TMPRSS2*, T2 inflammation,

447   whether observed *in vivo* or induced with IL-13 stimulation, precipitated a dramatic

448   reduction in levels of epithelial *ACE2*, thus complicating expectations for how T2

449   inflammation might affect overall risk for a poor COVID-19 outcome. Germane to this

450   question, a recent study of 85 fatal COVID-19 subjects found that 81.2% of them

451   exhibited very low levels of blood eosinophil levels[4]. Blood eosinophil levels are a

452   strong, well-known predictor of airway T2 inflammation and were strongly correlated

453   with T2 status in our study as well[11, 23]. Together, these studies provisionally suggest

454   that T2 inflammation may predispose individuals to experience better COVID-19

455   outcomes through a decrease in airway levels of *ACE2* that override any countervailing

456   effect from increased expression of *TMPRSS2*. However, both *in vitro* experiments

457   examining IL-13 effects on SARS-CoV-2 infection and empirical data on COVID-19

458   outcomes among T2-high and T2-low patients will certainly be needed to determine

459   whether this common airway inflammatory endotype ultimately protects against or

460   exacerbates COVID-19 illness. As mentioned above, we note that measurement of

461   blood eosinophil levels could be used as an informative and more accessible (albeit less

462   powerful) proxy for investigating the association between airway T2 inflammation and

463   outcomes of COVID-19. Moreover, given the higher frequency of T2 inflammation

464   among asthmatic subjects, this population should be monitored especially closely given

465   the enhanced risk of complications due to respiratory virus infection in those with

466   asthma.

467

468   In addition to a strong negative influence of T2 inflammation on *ACE2* expression in the

469   airway, we found an equally strong positive influence of respiratory virus infections on

470   levels of this gene. Network analysis placed *ACE2* within an interferon viral response

471   network suggesting that these cytokines are a driving force behind *ACE2* upregulation.

472   This information is interesting in several regards. First, it suggests that SARS-CoV-2

473   and other coronaviruses using ACE2 as a receptor could leverage the host anti-viral

474   response to increase the infectability of airway cells. Secondly, as data here and

475   elsewhere show, asymptomatic carriage of respiratory viruses is common, especially in

476   young children[19, 28-31]. Children in the GALA II cohort included in this study ranged in

477   age from 8-21 years; among them we found 18% who were carrying respiratory viruses

478   without illness. However, as we show in this and our previous study[19], even

479   asymptomatic carriage of respiratory viruses exacts a fundamental change in airway

480   epithelial expression and immune cell presence, including upregulation of *ACE2*

481   expression. In determining outcomes, this potential detrimental influence of virus

482   carriage may also be weighed against a potentially beneficial influence of virus carriage

483   through a more potent cross serologic-immune defense in these individuals, especially if

484   the virus carried is a coronavirus family member. Ultimately, the effect of current or

485   recent virus carriage on COVID-19 outcomes will need to be determined by *in vivo*

486   studies in patients, followed up with controlled *in vitro* studies of virally infected cells. At

487   any rate, the apparent dependence of *ACE2* expression on interferon signaling

488   suggests that targeted blockade of this interferon effect could control SARS-CoV-2

489   infection.

490

491   Our evaluation of genetic influences on airway *ACE2* and *TMPRSS2* expression

492   revealed a single rare eQTL for *ACE2* and several more frequent eQTL variants for

493   *TMPRSS2*. While both the effect size and explanatory power of these variants paled in

494   comparison to the influence of T2 inflammation and interferon signaling in multi-variable

495   modeling of expression for these genes, the effect of these variants may still be strong

496   enough to alter infection rates and or illness severity, especially in the populations

497   where these variants are most frequent. Thus, future genetic studies of COVID-19

498   should pay particular attention to these eQTL variants.

499

500   A particularly vexing question regards the mechanisms that underlie the unusual

501   severity of illness associated with SARS-CoV-2, especially when compared to most

502   circulating respiratory viruses. Clearly, severe disease often entails development of

503   pneumonia, possibly resulting from an expanded tropism of SARS-CoV-2 to include

504   lower lung airway and alveolar cells. The most severe patients also appear to

505   experience an exuberant immune response, characterized a "cytokine storm"[24],

506   occurring with and possibly driving the development of acute respiratory distress

507   syndrome (ARDS). Supposing that aspects of epithelial response to coronavirus family

508   members would be shared, including with SARS-CoV-2, we examined *in vivo*

509   coronavirus infection among the GALA II children. We found that CoV infections elicit a

510   broad airway transcriptome response, similar to HRV infections, and we identified a

511   panel of cytokines and transcription factors that likely regulate these responses. In

512   particular, we found that IL-6 was predicted to regulate responses to CoV and was itself

513   upregulated with these infections. These data support the recent investigation of

23

514   tocilizumab (IL-6R blocking antibody) for the treatment of COVID-19 illnesses[24].

515   Strikingly our analysis revealed an increased cytotoxic immune response with CoV

516   infection, driven by the differential presence and activity of cytotoxic CD8+ T cells and

517   NK cells, as compared to the more heavily neutrophil-based responses to HRV

518   infection. Although preliminary, this finding, if similarly occurring with SARS-CoV-2

519   infection, could partly explain the dramatic inflammation observed in SARS-CoV-2

520   patients, which can extend to the distal lung.

521

522   In summary, our data suggests that the strongest determinants of airway *ACE2* and

523   *TMPRSS2* expression are T2 inflammation and viral-induced interferon inflammation,

524   with limited but noteworthy influence from genetic variation. Whether these factors drive

525   better or worse clinical outcomes remains to be determined, but closely watching

526   individuals with these airway endotypes in the clinical management of COVID-19

527   illnesses would be prudent.

528

529

530

531

532

533

534

535

536

537   *Methods*

538

539   MATERIALS AND CORRESPONDENCE

540   Further information and requests for resources and reagents should be directed to and

541   will be fulfilled by Max A. Seibold, Ph.D. (seiboldm@njhealth.org)

542

543   EXPERIMENTAL METHODS

544

545   **Human subject information**

546   Under the Institutional Review Board (IRB) approved Asthma Characterization Protocol

547   (ACP) at National Jewish Health (HS-3101) we consented a 56 year old asthmatic

548   subject, from which we collected nasal airway epithelial cells. The nasal airway cells

549   were brushed from the inferior turbinate using a cytology brush and used for the scRNA-

550   seq experiment described in Figure 1. Nasal airway epithelial cells used for bulk RNA-

551   seq network and eQTL analysis came from GALA II study subjects described below.

552   Nasal airway epithelial cell ALI culture experiments all used cells derived from GALA II

553   study subjects. Human tracheal airway epithelial cells used for *in vitro* IL13 stimulation

554   and scRNA-seq experiment were isolated from a single de-identified lung donor

555   obtained from the International Institute for the Advancement of Medicine (Edison, NJ),

556   and Donor Alliance of Colorado. The National Jewish Health Institutional Review Board

557   (IRB) approved our research on the tracheal airway epithelial cells under IRB protocol

558   HS-3209. These cells were processed and given to us through the National Jewish

25

559   Health (NJH) live cell core, which is an institutional review board-approved study (HS-

560   2240) for the collection of tissues from consented patients for researchers at NJH.

561

562   **GALA II study subjects**

563   The Genes-Environment & Admixture in Latino Americans study (GALA II) is an on-

564   going case-control study of asthma in Latino children and adolescents. GALA II was

565   approved by local institutional review boards (UCSF, IRB number 10–00889, Reference

566   number 153543, NJH HS-2627) and all subjects and legal guardians provided written

567   informed assent and written informed consent, respectively[32, 33]. A full description of the

568   study design and recruitment has been previously described elsewhere[32-34]. Briefly, the

569   study includes subjects with asthma and healthy controls of Latino descent between the

570   ages of 8 and 21, recruited from the community centers and clinics in the mainland U.S.

571   and Puerto Rico (2006-present). Asthma case status was physician-diagnosed.

572   Recruited   subjects   completed   in-person   questionnaires   detailing   medical,

573   environmental,   and   demographic   information.   Physical   measurements   including

574   spirometry were obtained, and subjects provided a blood sample for DNA extraction and

575   later Whole Genome Sequencing. GALA subjects that were part of this analysis were all

576   recruited from Puerto Rico (n=695). A nasal airway inferior turbinate brushing was used

577   to collect airway epithelial cells from these subjects for whole transcriptome sequencing

578   (n=695). Network analyses were performed on all subjects with nasal brushing whole

579   transcriptome sequencing data (n=695) and eQTL analysis was performed on the

580   subset (n=681) with whole genome sequencing generated genotype data.

581

582

Bulk RNA sequencing of GALA II and ALI Samples

Total RNA was isolated from GALA II subject nasal airway epithelial brushings using the AllPrep DNA/RNA Mini Kit (QIAGEN, Germantown, MD). Whole transcriptome libraries were constructed using the KAPA Stranded mRNA-seq library kit (Roche Sequencing and Life Science, Kapa Biosystems, Wilmington, MA) from 250ng of total input RNA with the Beckman Coulter Biomek FX^P automation system (Beckman Coulter, Fullerton, CA) according to the manufacturers protocol. Barcoded libraries were pooled and sequenced using 125bp paired-end reads on the Illumina HiSeq 2500 system (Illumina, San Diego, CA). Bulk RNA-seq data for the nasal and tracheal ALI cultures to measure *ACE2* and *TMPRSS2* levels reported in Figures 3b,c and 4g,h, was generated with KAPA Hyperprep Stranded mRNA-seq library kits (Roche Sequencing and Life Science, Kapa Biosystems, Wilmington, MA) and sequenced with a Novaseq 6000 using 150bp paired end reads.

596

597

Whole genome sequencing of GALA II Samples

Genomic DNA was extracted from whole blood obtained from GALA II study subjects using the Wizard Genomic DNA Purification kits (Promega, Fitchburg, WI), and DNA was quantified by fluorescent assay. DNA samples were sequenced as part of the Trans☐Omics for Precision Medicine (TOPMed) whole genome sequencing (WGS) program[35]. WGS was performed at the New York Genome Center and the Northwest Genomics Center on a HiSeqX system (Illumina, San Diego, CA) using a paired☐end

605　read length of 150 base pairs, to a minimum of 30X mean genome coverage. Details on

606　DNA sample handling, quality control, library construction, clustering and sequencing,

607　read processing, and sequence data quality control are described elsewhere[35]. Variant

608　calls were obtained from TOPMed data freeze 8 variant call format files.

609

610

611　**Experiments using an air-liquid interface, mucociliary culture system**

612　Primary human basal airway epithelial cells were expanded and differentiated at air-

613　liquid interface (ALI) *in vitro* according to established protocols[36]. Paired tracheal ALI

614　cultures were mock-treated or treated with 10 ng/mL IL-13 in media (20 µL apical; 500

615　µL basolateral) for the final 10 days of differentiation (ALI days 11-21) before harvest

616　and scRNA-seq analysis. In contrast, nasal ALI cultures used for bulk RNA-seq analysis

617　(N = 5 GALA II subjects) were either stimulated with IL-13 for 72h following completion

618　of mucociliary differentiation (25 days) or were infected with human rhinovirus strain

619　A16 for 4 h during the final 24 h of the 28 days of differentiation. Control cultures were

620　only treated with media.

621

622　**Preparation of ALI cultures for 10X scRNAseq**

623　Following stimulation experiments involving the tracheal airway epithelial ALI samples,

624　apical culture chambers were washed once with PBS and once with PBS supplemented

625　with dithiothreitol (DTT;10mM), followed by two PBS washes to remove residual DTT.

626　Cold active protease (CAP) solution (*Bacillus licheniformis* protease 2.5 µg/mL, DNase

627　125 U/mL, and 0.5 mM EDTA in DPBS w/o $Ca^{2+}Mg^{2+}$) was added to apical culture

628   chamber and incubated on ice for 10 minutes with mixing every 2.5 minutes.

629   Dissociated cells in CAP solution were added to 500 µL cold FBS, brought up to 5 mL

630   with cold PBS, and centrifuged at 225 x g and 4°C for 5 minutes. The cell pellet was

631   resuspended in 1 mL cold PBS+DTT, centrifuged at 225 x g and 4°C for 5 minutes, and

632   then washed twice with cold PBS. The final cell pellet was resuspended in PBS with

633   0.04% BSA for single cell gene expression profiling with the 10X Genomics system.

634   Sample capture, cDNA synthesis, and library preparation for 10d IL-13 ALI stimulations

635   was performed using protocols and reagents for 10X Genomics Chromium Single Cell

636   3' v3 kit. Single cell libraries were pooled for sequencing on an Illumina NovaSeq 6000.

637

638   **Nasal brush 10X scRNA-seq**

639   Nasal brush cells were dissociated from the brush using *Bacillus licheniformis* cold

640   active protease (10mg/ml), EDTA (0.5mM), and EGTA (0.5mM) at 4°C with vortex

641   mixing, followed by enzyme neutralization with FBS. Red blood cell lysis was

642   performed and cells were washed twice in 0.04% BSA/PBS. Cell concentration was

643   adjusted to 400 cells/µL for cell capture of ~8000 cells using the 10X Genomics

644   Chromium Next GEM Single Cell 3' reagent kit chemistry. Sample capture, cDNA

645   synthesis, and library preparation was performed following 10X Genomics Chromium

646   Next GEM Single Cell 3' v3 kit. The single cell library was sequenced on an Illumina

647   NovaSeq 6000.

648

649   QUANTIFICATION AND STATISTICAL ANALYSIS

650

651 **Nasal airway epithelium brushing bulk RNA-seq analysis**

652

653 *Preprocessing of RNA-seq data*

654 Raw sequencing reads were trimmed using skewer[37] (v0.2.2) with the following

655 parameter settings: end-quality=15, mean-quality=25, min=30. Trimmed reads were

656 then aligned to the human reference genome GRCh38 using GSNAP[38] (v20160501)

657 with the following parameter settings: max-mismatches=0.05, indel-penalty=2, batch=3,

658 expand-offsets=0, use-sarray=0, merge-distant-same-chr. Gene quantification was

659 performed with htseq-count[39] (v0.9.1) using iGenomes GRCh38 gene transcript model.

660 Variance stabilization transformation (VST) implemented in DESeq2[40] (v1.22.2) was

661 then carried out on the raw gene count matrix to create a variance stabilized gene

662 expression matrix suitable for downstream analyses.

663

664 *Weighted Gene Co-expression Network Analysis (WGCNA) on GALA II RNA-seq data*

665 To understand what biological mechanisms regulate the variation of nasal airway

666 epithelial gene expression, Weighted Gene Co-expression Network Analysis[41]

667 (WGCNA) v1.68 was performed on the VST matrix of 17,473 expressed genes.

668 WGCNA analysis is a network-based approach that assumes a scale-free network

669 topology. To adhere to the scale-free assumption of the constructed biological networks,

670 a soft thresholding parameter (ß) value of 9 was chosen based on WGCNA guidelines.

671 Furthermore, minClusterSize was set to 20, deepSplit was set to 2, and pamStage was

672 set to TRUE. A total of 54 co-expression networks were identified and described in

673 Supplementary Table 2. WGCNA networks are referred to by different colors, and two of

30

674   the these identified networks, saddle brown and tan were found to capture co-

675   expressed genes that underlie T2 inflammation and interferon inflammation,

676   respectively. We hierarchically clustered all subjects based on expression of genes in

677   the saddle brown network and then used the first split in the dendrogram as the basis

678   for assigning individuals to T2-high or T2-low categories (Supplementary Figure 1a).

679   Similarly, we hierarchically clustered subjects using the genes in tan network and then

680   selected the dendrogram branches with the highest tan network expression as

681   interferon-high and the other subjects as interferon-low (Supplementary Figure 2a).

682

683   *Cis-eQTL analysis of nasal RNA-seq data*

684   Cis-expression quantitative trait locus (eQTL) analysis was performed by following the

685   general methodology of the Genotype-Tissue Expression (GTEx) project version 7

686   protocol[42], using the nasal RNA-seq data and WGS variant data from 681 GALA II

687   subjects.

688   Namely, WGS variant data was filtered based on allele frequency (minor allele

689   frequency > 1%) and allele subject count (total number of subjects carrying minor allele

690   ≥ 10). After filtering, 12,590,800 genetic variants were carried forward into the eQTL

691   analysis. For expression data filtering and preparation, we first ran Kallisto[43] (v0.43.0) to

692   generate transcript per million (TPM) values. We filtered out any genes that did not

693   reach both TPM > 0.1 and raw counts > 6 for at least 20% of our samples. After filtering,

694   17,039 genes were then TMM normalized using edgeR[44] (v3.22.3). Finally, we applied

695   an inverse normal transformation into the TMM-normalized expression values to render

696   them suitable for eQTL analysis. To account for global population structure, we ran

697 ADMIXTURE[45] (v1.3.0) on the genotype data to create five admixture factors. We then

698 ran Probabilistic Estimation of Expression Residuals[46] (PEER, v1.3) to create 60 PEER

699 factors to utilize as covariates in the eQTL analysis along with admixture estimates,

700 gender, age, body-mass index (BMI), and asthma diagnosis status. To perform cis-

701 eQTL analysis, we utilized a modified version of FastQTL[47] that was provided by the

702 GTEx project. Furthermore, we performed stepwise regression analysis to identify

703 independent eQTL variants using QTLTools[48] (v1.1). Allelic Fold Change (A_{FC}) of the

704 eQTL variant is computed using the aFC python script[49].

705

706 *Virus identification and quantification from bulk RNA-Seq data*

707 To identify individuals with asymptomatic virus infection at the time of sample collection,

708 viral genomic sequences were recovered from bulk RNA-seq data using a modified

709 version of the Virus Finder 2.0 (VF2) pipeline[50]. A custom respiratory virus reference

710 database comprising >600k sequences was employed to improve specificity. Using

711 VF2, viral reads were garnered by removing human reads using Bowtie2[51] (default

712 settings) and selecting viral reads using BLAT[52] (minIdentity=80); contigs were

713 assembled using Trinity[53]; short (<200 bp) or low complexity (DUST score < 0.07)

714 contigs and contigs matching the human genome at a BLAST[54] e-value <0.05 were

715 discarded; the remaining contigs were classified using BLAST (e-value <0.05); read

716 counts were obtained by read mapping using BLAT (minIdentity=98). Of the 468 distinct

717 viral reference sequences detected by VF2, 7 were identified as erroneous and

718 removed. The remaining 461 matches were manually assigned viral serotypes and the

719 results aggregated with R.

720

Defining CoV and HRV infected groups and associated analysis

To ensure we selected subjects that were experiencing an active host response to a CoV infection, we examined the distribution of viral reads for the 18 CoV$^+$ infected subjects. We observed a clear break between the 7 subjects with the lowest viral read counts (<3,000 reads) and 11 subjects with the highest viral read counts (>60,000 reads). Therefore, we selected these 11 highly infected subjects for analysis of host responses to CoV infection. To generate a similar infection-control group, composed of subjects highly infected with a different virus species, we examined the 67 HRV infected subjects in GALA, enforcing a comparable lower bound of viral reads as with CoV, adjusting for the smaller HRV genome size. Specifically, HRV genomes are ~7,000 base pairs, whereas CoV genomes are ~30,000 base pairs, making the HRV genome ~25% of the size of the CoV genome. Therefore, we selected a cutoff of 15,000 viral reads for subjects to be included in the HRV$^+$ highly infected group. Therefore, we selected a cutoff of 15,000 viral reads for subjects to be included in the HRV$^+$ highly infected group (n=37) analyzed in Figure 6. All non-infected subjects (n=571), based on the Virus Finder analysis described above, were used as comparison group for the CoV$^+$ and HRV$^+$ groups.

In performing the CoV$^+$ and HRV$^+$ transcriptome-wide differential expression analyses, to account for the class imbalance of this experiment, log$_2$ count-normalized expression values in units of counts per million (calculated using edgeR v3.28.0) were passed to the function arrayWeights function in the limma[55] R package (3.42.0). limma-voom was then used to perform differential expression analysis on the count normalized

33

743   expression values between the CoV$^+$ and uninfected groups, as well as between the

744   HRV$^+$ and uninfected groups, controlling for age, gender, and asthma diagnosis status.

745   Genes were required to have an FDR adjusted p-value < 0.05, and an absolute log$_2$FC

746   > 0.5 to be considered significant. Based on these cutoffs, genes were classified as

747   being shared if they were significant in both comparisons, or as CoV$^+$–specfic or HRV$^+$–

748   specific if significant in only one comparison.

749

750   *Gene set enrichment analysis.*

751   To investigate enriched pathways within WGCNA networks (see Figure 2a) or within

752   genes differentially expressed in CoV$^+$ and/or HRV$^+$ infected subject groups (see Figure

753   6c and 6c), we used Enrichr[56] to test for gene overrepresentation of network genes

754   within a panel of annotated gene databases (Gene Ontology [GO] Biological Process

755   [BP] 2018, GO Molecular Function [MF] 2018, GO Cellular Component [CC] 2018,

756   Kyoto Encyclopedia of Genes and Genomes [KEGG] 2019 Human, and Reactome

757   2016). For cell type enrichments within WGCNA networks reported in Figure 2a, we

758   tested for overrepresentation of network genes within gene marker sets (FDR < 0.05)

759   for each of 35 epithelial and immune cell types inferred using scRNA-seq of human lung

760   tissue[57].

761

762   For the plots in Figure 6f-g, transcriptomic data for 11 flow sorted immune cell

763   populations were obtained from GEO experiments GSE3982 and GSE22886 and then

764   batch corrected using the ComBat[58] function from the SVA R package (v3.34.0). limma

765   was then used to perform differential expression analysis between each cell type and all

766   the rest in order to obtain gene $\log_2$FC values for each cell type with which to rank order

767   the genes. Gene set enrichment analysis (GSEA) was then used to test for association

768   between upregulated genes in the shared, CoV⁺–specific, and HRV⁺–specific gene sets

769   and each of the cell types, based on the cell type-specific ordered gene lists. GSEA was

770   carried out using the FGSEA R package (v1.12.0).

771

772

773   *Canonical pathway analysis.*

774   We used QIAGEN's Ingenuity Pathway Analysis (IPA) program (v01-16; content

775   version: 51963813, release 2020-03-11) to investigate canonical pathways and

776   upstream regulators that were significantly enriched in one or both of the upregulated

777   CoV⁺-specific or HRV⁺-specific gene sets.

778

779   **Analysis of scRNA-seq data from the nasal epithelial brushing**

780   Initial processing of 10X scRNA-seq data, including cell demultiplexing, alignment to the

781   human genome GRCh38, and UMI-based quantification was performed with Cell

782   Ranger (version 3.0). Since the nasal brushing sample contains both epithelial and

783   immune cell populations that have distinct expression profiles (e.g.: Immune cell types

784   express far fewer genes compared to epithelial cell types), clustering and cell type

785   identification were done in two stages: 1) an initial clustering with a less stringent filter to

786   identify major epithelial and immune cell clusters was performed, 2) cells were

787   reclustered with different independent filtering criteria for epithelial and immune cell

788   types. All these analyses were performed using Seurat[59] R package (v3.0).

35

789

790   In the first stage, we removed cells with fewer than 100 genes detected or cells with

791   greater than 25% mitochondrial reads. Additionally, to remove possible doublets, we

792   removed cells with higher than 6,000 genes detected and/or more than 20,000 UMIs.

793   Lowly expressed genes (detected in fewer than 4 cells) were also removed. We then

794   performed normalization using SCTransform[60] and ran PCA on the top 5000 highly

795   variable normalized genes. Clustering analysis was performed on the top 20 PCs using

796   a shared nearest neighbor (SNN) based SLM[61] algorithm with the following parameter

797   settings: resolution=0.8, algorithm=3. The single cell expression profiles were visualized

798   via embedding into two dimensions with UMAP[62] (Uniform Manifold Approximation and

799   Projection), resulting in the identification of 11,157 epithelial cells and 229 immune cells

800   based on known cell type signatures.

801

802   In the second stage, we retained all the immune cells but removed epithelial cells with

803   fewer than 1,000 detected genes. After this filtering, a combined 8,291 epithelial and

804   immune cells were then normalized as in the first stage. Clustering analysis performed

805   on the top 30 PCs with parameters (resolution=0.4, algorithm=1, k.param=10) identified

806   15 clusters. We then ran differential expression analysis using a Wilcoxon test

807   implemented in Seurat's "FindMarkers" function to help with cell type identification.

808   Based on these cluster marker lists, two clusters were merged into a single secretory

809   cluster, another two clusters were merged into a single ciliated cluster, and a final two

810   clusters were combined as "indeterminate," based on the lack of defining marker genes

811   for these clusters. Through this merging process, we arrived at 8 epithelial and 3

812   immune cell populations (Figure 1a, Supplementary Table 1)

813

814

815   **Analysis of bulk RNA-seq data from IL-13 and HRV infected ALI nasal airway**

816   **epithelial cultures**

817   Raw sequencing reads were trimmed using skewer with the following parameter

818   settings: end-quality=15, mean-quality=25, min=30. Trimmed reads were then aligned to

819   the human reference genome GRCh38 using HISAT2[63] (v2.1.0) using default parameter

820   settings. Gene quantification was performed with htseq-count using the GRCh38

821   Ensembl v84 gene transcript model. After removing mitochondrial, ribosomal, and lowly

822   expressed genes (those not expressed in at least two samples), we carried out

823   differential expression analyses between paired IL-13-stimulated and control samples

824   (N = 5 donors) and between paired HRV-infected and control samples (N = 5 donors)

825   using the DESeq2 R package (v1.22.2).

826

827   **Analysis of scRNA-seq data from 10 day IL-13-stimulated and control tracheal cell**

828   **ALI cultures**

829   As with the nasal brushing scRNA-seq data, 10X scRNA-seq data from ALI cultures

830   grown from a single tracheal donor that were either mock- or IL-13 stimulated for 10

831   days were pre-processed using Cell Ranger (version 3.0, 10X Genomics). To safeguard

832   against doublets, we removed all cells with gene or UMI counts exceeding the 99th

833   percentile. We also removed cells expressing fewer than 1,500 genes or for which >

834   30% of genes were mitochondrial (genes beginning with *MTAT*, *MT-*, *MTCO*, *MTCY*,

835   *MTERF, MTND, MTRF, MTRN, MRPL,* or *MRPS*), resulting in a total of 6,969 cells

836   (2,715 IL-13-stimulated and 4,254 controls). After removing mitochondrial, ribosomal

837   (*RPL* and *RPS*), and very lowly expressed genes (expressed in < 0.1% of cells), we

838   integrated expression data from IL-13 and control cells using the dataset integration

839   approach in Seurat[64]. For the integration analysis, we used the top 30 dimensions from

840   a canonical correlation analysis (CCA) based on SCTransform normalized expression of

841   the top 3,000 most informative genes across the two datasets, where "informativeness"

842   was defined by gene dispersion (i.e., the log of the ratio of expression variance to its

843   mean) across cells, calculated after accounting for its relationship with mean

844   expression. We then carried out principle component analysis (PCA) on the integrated

845   dataset and used the top 20 components for clustering and visualization. We used SNN

846   (Louvain algorithm, resolution=0.23, k.param=10) to cluster the integrated cells into 11

847   populations, which we visualized in two dimensions using UMAP (see Figure 3d). These

848   clusters were assigned cell type labels based their most upregulated genes, which were

849   identified by carrying out differential expression analysis between each cluster and all

850   others using Seurat's logistic regression (LR) test, in which cell treatment was included

851   as a latent variable.

852

853   DATA AVAILABILITY

854   All raw and processed RNA-seq data used in this study are currently being deposited in

855   the National Center for Biotechnology Information/Gene Expression Omnibus (GEO).

856

857   CODE AVAILABILITY

858

859

860

861

862

863

864   *References*

865

866   1.   Wang, C., Horby, P.W., Hayden, F.G. & Gao, G.F. A novel coronavirus outbreak

867   of global health concern. *Lancet* **395**, 470-473 (2020).

868   2.   Zhu, N. *et al.* A Novel Coronavirus from Patients with Pneumonia in China, 2019.

869   *N Engl J Med* **382**, 727-733 (2020).

870   3.   Baud, D. *et al.* Real estimates of mortality following COVID-19 infection. *Lancet*

871   *Infect Dis* (2020).

872   4.   Du, Y. *et al.* Clinical Features of 85 Fatal Cases of COVID-19 from Wuhan: A

873   Retrospective Observational Study. *Am J Respir Crit Care Med* (2020).

874   5.   Zhou, F. *et al.* Clinical course and risk factors for mortality of adult inpatients with

875   COVID-19 in Wuhan, China: a retrospective cohort study. *Lancet* **395**, 1054-1062

876   (2020).

877   6.   Dong, Y. *et al.* Epidemiological Characteristics of 2143 Pediatric Patients With

878   2019 Coronavirus Disease in China. *Pediatrics* (2020).

879   7.   Hoffmann, M. *et al.* SARS-CoV-2 Cell Entry Depends on ACE2 and TMPRSS2

880   and Is Blocked by a Clinically Proven Protease Inhibitor. *Cell* (2020).

881   8.   Goldfarbmuren, K.C. *et al.* Dissecting the cellular specificity of smoking effects

882   and reconstructing lineages in the human airway epithelium. *Nature*

883   *Communications* **in press** (2020).

884   9.   Montoro, D.T. *et al.* A revised airway epithelial hierarchy includes CFTR-

885   expressing ionocytes. *Nature* **560**, 319-324 (2018).

886   10.   Plasschaert, L.W. *et al.* A single-cell atlas of the airway epithelium reveals the

887   CFTR-rich pulmonary ionocyte. *Nature* **560**, 377-381 (2018).

888   11.   Woodruff, P.G. *et al.* T-helper Type 2-driven inflammation defines major

889   subphenotypes of asthma. *American Journal of Respiratory and Critical Care*

890   *Medicine* **180**, 388-395 (2009).

891   12.   Barcelo, B. *et al.* Intracellular cytokine profile of T lymphocytes in patients with

892   chronic obstructive pulmonary disease. *Clinical and Experimental Immunology*

893   **145**, 474-479 (2006).

894   13.   George, L. & Brightling, C.E. Eosinophilic airway inflammation: role in asthma

895   and chronic obstructive pulmonary disease. *Therapeutic Advances in Chronic*

896   *Disease* **7**, 34-51 (2016).

897   14.   Chen, G. *et al.* SPDEF is required for mouse pulmonary goblet cell differentiation

898   and regulates a network of genes associated with mucus production. *Journal of*

899   *Clinical Investigation* **119**, 2914-2924 (2009).

900   15.   Lachowicz-Scroggins, M.E. *et al.* Abnormalities in MUC5AC and MUC5B protein

901   in airway mucus in asthma. *American Journal of Respiratory and Critical Care*

902   *Medicine* **194**, 1296-1299 (2016).

903   16.   de Lamballerie, C.N. *et al.* Characterization of cellular transcriptomic signatures

904   induced by different respiratory viruses in human reconstituted airway epithelia.

905   *Scientific Reports* **9** (2019).

906   17.   Steuerman, Y. *et al.* Dissection of influenza infection *in vivo* by single-cell RNA

907   sequencing. *Cell Systems*, 679-691 (2018).

908   18.   Terrier, O. *et al.* Cellular transcriptional profiling in human lung epithelial cells

909   infected by different subtypes of influenza A viruses reveals an overall down-

910   regulation of the host p53 pathway. *Virology Journal* **8** (2011).

911   19.   Wesolowska-Andersen, A. *et al.* Dual RNA-seq reveals viral infections in

912   asthmatic children without respiratory illness which are associated with changes

913   in the airway transcriptome. *Genome Biology* **18**, 1:17 (2017).

914   20.   Aguet, F. *et al.* Genetic effects on gene expression across human tissues. *Nature*

915   **550**, 204-217 (2017).

916   21.   Everman, J.L. *et al.* Functional genomics of CDHR3 confirms its role in HRV-C

917   infection and childhood asthma exacerbations. *Journal of Allergy and Clinical*

918   *Immunology* **144**, 962-971 (2019).

919   22.   Caliskan, M. *et al.* Rhinovirus wheezing illness and genetic risk of childhood-

920   onset asthma. *New England Journal of Medicine* **368**, 1398-1407 (2013).

921   23.   Poole, A. *et al.* Dissecting childhood asthma with nasal transcriptomics

922   distinguishes subphenotypes of disease. *J Allergy Clin Immunol* **133**, 670-678

923   e612 (2014).

924   24.   Mehta, P. *et al.* COVID-19: consider cytokine storm syndromes and

925   immunosuppression. *Lancet* **395**, 1033-1034 (2020).

926   25.   Lukassen S, C.R., Elis R SARS-CoV-2 receptor ACE2 and TMPRSS2 are

927   predominantly expressed in a transient secretory cell type in subsegmental

928   bronchial branches. *biorxiv* (2020).

929   26.   Kesic, M.J., Meyer, M., Bauer, R. & Jaspers, I. Exposure to ozone modulates

930   human airway protease/antiprotease balance contributing to increased influenza

931   A infection. *PLoS One* **7**, e35108 (2012).

932   27.   Peters, M.C. *et al.* A Transcriptomic Method to Determine Airway Immune

933   Dysfunction in T2-High and T2-Low Asthma. *Am J Respir Crit Care Med* **199**,

934   465-477 (2019).

935   28.   Advani, S., Sengupta, A., Forman, M., Valsamakis, A. & Milstone, A.M. Detecting

936   respiratory viruses in asymptomatic children. *Pediatr Infect Dis J* **31**, 1221-1226

937   (2012).

938   29.   Jartti, T., Jartti, L., Peltola, V., Waris, M. & Ruuskanen, O. Identification of

939   respiratory viruses in asymptomatic subjects: asymptomatic respiratory viral

940   infections. *Pediatr Infect Dis J* **27**, 1103-1107 (2008).

941   30.   Singleton, R.J. *et al.* Viral respiratory infections in hospitalized and community

942   control children in Alaska. *J Med Virol* **82**, 1282-1290 (2010).

943   31.   Stelzer-Braid, S. *et al.* Absence of back to school peaks in human rhinovirus

944   detections and respiratory symptoms in a cohort of children with asthma. *J Med*

945   *Virol* **88**, 578-587 (2016).

946   32.   Neophytou, A.M. *et al.* Air Pollution and Lung Function in Minority Youth with

947   Asthma in the GALA II (Genes-Environments and Admixture in Latino

948   Americans) and SAGE II (Study of African Americans, Asthma, Genes, and

949   Environments) Studies. *Am J Respir Crit Care Med* **193**, 1271-1280 (2016).

950   33.   Nishimura, K.K. *et al.* Early-life air pollution and asthma risk in minority children.

951   The GALA II and SAGE II studies. *Am J Respir Crit Care Med* **188**, 309-318

952   (2013).

953   34.   Thakur, N. *et al.* Socioeconomic status and childhood asthma in urban minority

954   youths. The GALA II and SAGE II studies. *Am J Respir Crit Care Med* **188**, 1202-

955   1209 (2013).

956   35.   Taliun, D. *et al.* Sequencing of 53,831 diverse genomes from the NHLBI

957   TOPMed Program. *bioRxiv* (2019).

958   36.   Everman, J.L., Rios, C. & Seibold, M.A. Utilization of Air-Liquid Interface Cultures

959   as an In Vitro Model to Assess Primary Airway Epithelial Cell Responses to the

960   Type 2 Cytokine Interleukin-13. *Methods Mol Biol* **1799**, 419-432 (2018).

961   37.   Jiang, H., Lei, R., Ding, S.W. & Zhu, S. Skewer: a fast and accurate adapter

962   trimmer for next-generation sequencing paired-end reads. *BMC Bioinformatics*

963   **15**, 182 (2014).

964   38.   Wu, T.D. & Nacu, S. Fast and SNP-tolerant detection of complex variants and

965   splicing in short reads. *Bioinformatics* **26**, 873-881 (2010).

966   39.   Anders, S., Pyl, P.T. & Huber, W. HTSeq--a Python framework to work with high-

967   throughput sequencing data. *Bioinformatics* **31**, 166-169 (2015).

968   40.   Love, M.I., Huber, W. & Anders, S. Moderated estimation of fold change and

969   dispersion for RNA-seq data with DESeq2. *Genome Biol* **15**, 550 (2014).

970   41.   Langfelder, P. & Horvath, S. WGCNA: an R package for weighted correlation

971   network analysis. *BMC Bioinformatics* **9**, 559 (2008).

972   42.   Consortium, G.T. *et al.* Genetic effects on gene expression across human

973   tissues. *Nature* **550**, 204-213 (2017).

974   43.   Bray, N.L., Pimentel, H., Melsted, P. & Pachter, L. Near-optimal probabilistic

975   RNA-seq quantification. *Nat Biotechnol* **34**, 525-527 (2016).

976   44.   Robinson, M.D., McCarthy, D.J. & Smyth, G.K. edgeR: a Bioconductor package

977   for differential expression analysis of digital gene expression data. *Bioinformatics*

978   **26**, 139-140 (2010).

979   45.   Alexander, D.H. & Lange, K. Enhancements to the ADMIXTURE algorithm for

980   individual ancestry estimation. *BMC Bioinformatics* **12**, 246 (2011).

981   46.   Stegle, O., Parts, L., Durbin, R. & Winn, J. A Bayesian framework to account for

982   complex non-genetic factors in gene expression levels greatly increases power in

983   eQTL studies. *PLoS Comput Biol* **6**, e1000770 (2010).

984   47.   Ongen, H., Buil, A., Brown, A.A., Dermitzakis, E.T. & Delaneau, O. Fast and

985   efficient QTL mapper for thousands of molecular phenotypes. *Bioinformatics* **32**,

986   1479-1485 (2016).

987   48.   Delaneau, O. *et al.* A complete tool set for molecular QTL discovery and

988   analysis. *Nat Commun* **8**, 15452 (2017).

989   49.   Mohammadi, P., Castel, S.E., Brown, A.A. & Lappalainen, T. Quantifying the

990   regulatory effect size of cis-acting genetic variation using allelic fold change.

991   *Genome Res* **27**, 1872-1884 (2017).

992   50.   Wang, Q., Jia, P. & Zhao, Z. VERSE: a novel approach to detect virus integration

993   in host genomes through reference genome customization. *Genome Med* **7**, 2

994   (2015).

995   51.   Langmead, B. & Salzberg, S.L. Fast gapped-read alignment with Bowtie 2. *Nat*

996   *Methods* **9**, 357-359 (2012).

997   52.   Kent, W.J. BLAT--the BLAST-like alignment tool. *Genome Res* **12**, 656-664

998   (2002).

999   53.   Grabherr, M.G. *et al.* Full-length transcriptome assembly from RNA-Seq data

1000   without a reference genome. *Nat Biotechnol* **29**, 644-652 (2011).

1001   54.   Altschul, S.F., Gish, W., Miller, W., Myers, E.W. & Lipman, D.J. Basic local

1002   alignment search tool. *J Mol Biol* **215**, 403-410 (1990).

1003   55.   Ritchie, M.E. *et al.* limma powers differential expression analyses for RNA-

1004   sequencing and microarray studies. *Nucleic Acids Res* **43**, e47 (2015).

1005   56.   Chen, E.Y. *et al.* Enrichr: interactive and collaborative HTML5 gene list

1006   enrichment analysis tool. *BMC Bioinformatics* **14**, 128 (2013).

1007   57.   Travaglini, K.J. *et al.* A molecular cell atlas of the human lung from single cell

1008   RNA sequencing. *biorxiv* (2020).

1009   58.   Johnson, W.E., Li, C. & Rabinovic, A. Adjusting batch effects in microarray

1010   expression data using empirical Bayes methods. *Biostatistics* **8**, 118-127 (2007).

1011   59.   Butler, A., Hoffman, P., Smibert, P., Papalexi, E. & Satija, R. Integrating single-

1012   cell transcriptomic data across different conditions, technologies, and species.

1013   *Nat Biotechnol* **36**, 411-420 (2018).

1014   60.   Hafemeister, C. & Satija, R. Normalization and variance stabilization of single-cell

1015   RNA-seq data using regularized negative binomial regression. *Genome Biol* **20**,

1016   296 (2019).

1017   61.   Waltman, L. & Van Eck, N.J. A smart local moving algorithm for large-scale

1018   modularity-based community detection. *European Physical Journal B* **86**, 471

1019   (2013).

1020   62.   McInnes, L. & Healy, J. Uniform Manifold Approximation and Projection for

1021   Dimension Reduction. *ArXiv* (2018).

1022   63.   Kim, D., Langmead, B. & Salzberg, S.L. HISAT: a fast spliced aligner with low

1023   memory requirements. *Nat Methods* **12**, 357-360 (2015).

1024   64.   Stuart, T. *et al.* Comprehensive integration of single-cell data. *Cell* **177**, 1888-

1025   1902 (2019).

1026

1027

1028

1029

1030

1031

1032

1033   *Acknowledgements*

1034

1080   data: Duanny Alva, MD; Gaby Ayala-Rodríguez; Lisa Caine, RT; Elizabeth Castellanos;

1081   Jaime Colón; Denise DeJesus; Blanca López; Brenda López, MD; Louis Martos; Vivian

1082   Medina; Juana Olivo; Mario Peralta; Esther Pomares, MD; Jihan Quraishi; Johanna

1083   Rodríguez; Shahdad Saeedi; Dean Soto; and Ana Taveras.

1084   The content is solely the responsibility of the authors and does not necessarily

1085   represent the official views of the National Institutes of Health.

1086
1087

1088

1089

1090

1091

1092

1093

1094

1095

1096

1097

1098

1099

1100

1101

1102

1103

1104

1105

1106

1107

1108

1109

1110

1111 *Figure Legends*

1112

1113 **Figure 1. *ACE2* and *TMPRSS2* are expressed by multiple nasal airway epithelial**

1114 **cell types**

1115 (a) UMAP visualization of cells derived from a human nasal airway epithelial brushing

1116 depicts multiple epithelial and immune cell types identified through unsupervised

1117 clustering.

1118 (b) Normalized expression of *ACE2* in epithelial and immune cell types.

1119 (c) Normalized expression of *TMPRSS2* in epithelial and immune cell types.

1120

1121 **Figure 2. *TMPRSS2* is a mucus secretory network gene regulated by T2**

1122 **inflammation**

1123 (a) WGCNA identified networks of co-regulated genes related to mucus secretory

1124 function (black), T2 inflammation-induced mucus secretory function (pink), and

1125   canonical T2 inflammation biomarkers (saddle brown). *TMPRSS2* was within the pink

1126   network. Select pathway and cell type enrichments for network genes are shown.

1127   (b) Scatterplot revealing a strong positive correlation between *TMPRSS2* expression

1128   and summary (eigengene) expression of the T2 inflammatory, mucus secretory network.

1129   (c) Scatterplot revealing a strong positive correlation between *TMPRSS2* expression

1130   and summary (eigengene) expression of the canonical T2 inflammation biomarker

1131   network.

1132   (d) Box plots revealing strong upregulation of *TMPRSS2* expression among T2-high

1133   compared to T2-low subjects.

1134   (e) Scatterplot revealing a strong negative correlation between *ACE2* expression and

1135   summary (eigengene) expression of the T2 inflammation mucus secretory network.

1136   (f) Scatterplot revealing a strong negative correlation between *ACE2* expression and

1137   summary (eigengene) expression of the canonical T2 inflammation biomarker network.

1138   (g) Box plots revealing strong downregulation of *ACE2* expression among T2-high

1139   compared to T2-low subjects.

1140

1141   **Figure 3. *ACE2* and *TMPRSS2* expression are both regulated by IL-13 in the**

1142   **mucociliary airway epithelium**

1143   (a) Experimental schematic detailing the timeline for differentiation of basal airway

1144   epithelial cells into a mucociliary airway epithelium and treatment with chronic (10 days)

1145   or acute (72 hours) IL-13 (10ng/ml).

51

1146 (b) Box plots of count-normalized expression between paired nasal airway cultures

1147 (control/IL-13) revealing strong downregulation of bulk *ACE2* expression with IL-13

1148 treatment. Differential expression results are from DESeq2.

1149 (c) Box plots of count-normalized expression between paired nasal airway cultures

1150 (control/IL-13) revealing strong upregulation of bulk *TMPRSS2* expression with IL-13

1151 treatment. Differential expression results are from DESeq2.

1152 (d) UMAP visualization of cells derived from control and IL-13 stimulated tracheal airway

1153 ALI cultures depict multiple epithelial cell types identified through unsupervised

1154 clustering.

1155 (e) Violin plots of normalized *ACE2* expression across epithelial cell types from tracheal

1156 airway ALI cultures, stratified by treatment (gray = control, red = IL-13). Differential

1157 expression using a Wilcoxon test was performed between control and IL-13-stimulated

1158 cells with significant differences in expression for a cell type indicated by a * (p < 0.05).

1159 (f) Violin plots of normalized *TMPRSS2* expression across epithelial cell types from

1160 tracheal airway ALI cultures, stratified by treatment (gray = control, red = IL-13).

1161 Differential expression using a Wilcoxon test was performed between control and IL-13-

1162 stimulated cells with significant differences in expression for a cell type indicated by a *

1163 (p < 0.05).

1164

1165 **Figure 4. *ACE2* is an interferon response network gene regulated by respiratory**

1166 **virus infections**

1167 (a) Scatter plot revealing a strong positive correlation between *ACE2* expression and

1168 summary (eigengene) expression of the cytotoxic immune response network (purple).

1169　(b) Scatterplot revealing a strong positive correlation between *ACE2* expression and

1170　summary (eigengene) expression of the interferon response network (tan).

1171　 (c) WGCNA analysis identified networks of co-regulated genes related to cytotoxic

1172　immune response (purple) and interferon response (tan). *ACE2* was within the purple

1173　network. Select pathway and cell type enrichments for network genes are shown.

1174　(d) Box plots of count-normalized expression from GALA II nasal epithelial samples

1175　reveal strong upregulation of *ACE2* expression among interferon-high compared to

1176　interferon-low subjects. Differential expression results are from DESeq2.

1177　(e) Pie graph depicting the percentage of each type of respiratory virus infection found

1178　among GALA II subjects in whom viral reads were found.

1179　(f) Experimental schematic detailing timeline for differentiation of basal airway epithelial

1180　cells into a mucociliary airway epithelium and experimental infection with HRV-A16.

1181　(g) Box plots of count-normalized expression between paired nasal airway cultures

1182　(control/HRV-A16 infected) revealing strong upregulation of *ACE2* expression with

1183　HRV-A16 infection. Differential expression results are from DESeq2.

1184　(h) Box plots of count-normalized expression between paired nasal airway cultures

1185　(control/HRV-A16-infected) revealing no effect of HRVA-16 on *TMPRSS2* expression.

1186　Differential expression results are from DESeq2.

1187

1188　**Figure 5. *ACE2* and *TMPRSS2* nasal airway expression are regulated by eQTL**

1189　**variants**

1190　(a) Locuszoom plot of *ACE2* eQTL signals. The lead eQTL variant (rs18160331) is

1191　highlighted with a purple dot. The strength of Linkage Disequilibrium (LD) between

1192   rs18160331 and other variants is discretely divided into five quantiles and mapped into

1193   five colors (dark blue, sky blue, green, orange, and red) sequentially from low LD to high

1194   LD.

1195   (b) Locuszoom plot of *TMPRSS2* eQTL signals. The three independent eQTL variants

1196   (rs1475908, rs2838057, rs74659079) and their LD with other variants (r^2) are

1197   represented by red, blue, and green color gradient respectively.

1198   (c) Box plots of normalized *ACE2* expression among the three genotypes of the lead

1199   *ACE2* eQTL variant (rs18160331). $\log_2 A_{FC}$ = log2 of the allelic fold change associated

1200   with the variant.

1201   (d) Box plots of normalized *TMPRSS2* expression among the three genotypes of the

1202   lead *TMPRSS2* eQTL variant (rs1475908). $\log_2 A_{FC}$ = log2 of the allelic fold change

1203   associated with the variant.

1204   (e) Bar plots depicting allele frequencies of the *ACE2* eQTL variant rs18160331 and

1205   *TMPRSS2* eQTL variants (rs1475908, rs2838057, rs74659079) across world

1206   populations. Allele frequency data were obtained from gnomAD v2.1.1.

1207

1208   **Figure 6. Coronavirus infections elicit an enhanced cytotoxic immune response**

1209   **from the airway epithelium**

1210   (a) Box plots revealing a strong and equivalent upregulation of summary (eigengene

1211   [E_g]) expression for the interferon response network among HRV and CoV-infected

1212   GALA II subjects, compared to uninfected subjects.

1213 (b) Box plots revealing upregulation in summary (eigengene) expression for the

1214 cytotoxic immune response network among HRV-infected GALA II subjects that is even

1215 stronger for the CoV infected group.

1216 (c) Venn Diagram describing the number of differentially expressed genes in HRV and

1217 CoV infected groups compared to the uninfected group, and the extent of their overlap.

1218 For genes differentially expressed in both groups, select enriched pathways and

1219 underlying genes that are highly differentially expressed are shown.

1220 (d) Top upstream regulators predicted by Ingenuity Pathway Analysis to be regulating

1221 the genes that were upregulated in CoV. Enrichment values for these CoV regulators,

1222 using the HRV upregulated genes are also shown.

1223 (e) Heatmap of the $\log_2$FC in gene expression for CoV and HRV groups when

1224 compared to the uninfected group. Top significantly upregulated genes are shown,

1225 along with *ACE2*, *IL6*, and genes identified as belonging to cytotoxic pathways, which

1226 were enriched within the virally upregulated CoV group DEGs based on IPA canonical

1227 pathway analysis. Color bars indicate which WGCNA network and or IPA canonical

1228 pathway each gene belongs to.

1229 (f) Gene set enrichment analysis plot for CD8+ T cells. The black (shared), yellow (CoV-

1230 enhanced), and red (HRV-enhanced) curves display the enrichment score for the

1231 indicated viral gene set as the analysis walks down the ranked distribution of genes

1232 ordered by fold change in expression between CD8+ T cells relative to all other immune

1233 cell types (red-blue color bar). Genes are represented by vertical bars in the same color

1234 as the curve of the viral gene group they represent. Denoted genes are a representative

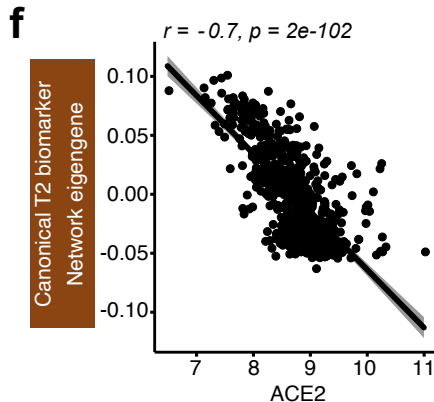1235 set from the leading edge (most responsible for the enrichment).

55

1236   (g) Gene set enrichment analysis plot for NK cells. The black (shared), yellow (CoV-

1237   enhanced), and red (HRV-enhanced) curves display the enrichment score for the

1238   indicated viral gene set as the analysis walks down the ranked distribution of genes

1239   ordered by fold change in expression between NK cells relative to all other immune cell

1240   types (red-blue color bar). Genes are represented by vertical bars in the same color as

1241   the curve of the viral gene group they represent. Denoted genes are from the leading

1242   edge (most responsible for the enrichment).

1243

1244

1245

a
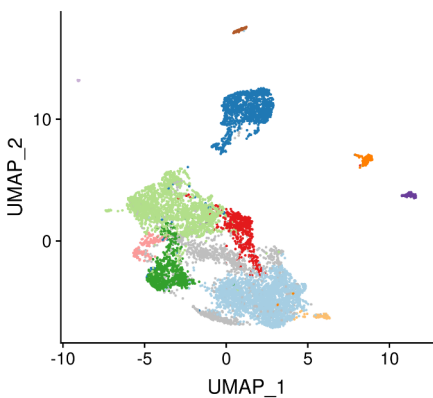
b ACE2
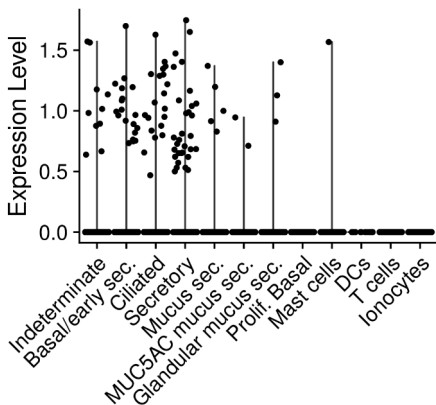
c TMPRSS2
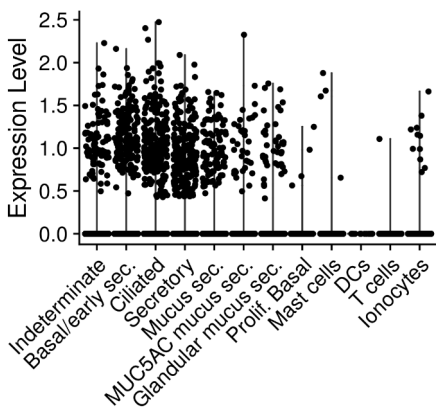
a

Network (color)	Network size (# genes)	Select genes	Pathway enrichment	Cell-type enrichment
Mucus secretory (black)	477	COPA COPB2 COPG1 CREB3L1 XBP1	Golgi vesicle transport (p-adj: 2e-6)	Goblet (p-adj: 2e-17)
			COPI-mediated anterograde transport (p-adj: 9e-6)	Diff. basal (p-adj: 0.03)
T2 mucus secretory (pink)	446	SPDEF FCGBP FOXA3 IL13 BPIFB1	O-glycan processing (p-adj: 9e-4)	Goblet (p-adj: 2e-6)
			Polypeptide N-acetylgalactosaminyltransferase activity (p-adj: 3e-3)	Serous (p-adj: 3e-3)
Canonical T2 biomarker (saddle brown)	156	CLCA1 CCL26 POSTN IL1RL1 CPA3	Interleukin-13 human airway epithelial cells (p-adj: 9e-29)	Mast cell/basophil type 1 (p-adj: 6e-11)
			Interleukin-4 human keratinocyte (p-adj: 0.02)	Mast cell/basophil type 2 (p-adj: 6e-11)

b $r = 0.68, p = 3e-97$

T2 mucus secretory Network eigengene vs TMPRSS2

c $r = 0.61, p = 5e-72$

Canonical T2 biomarker Network eigengene vs TMPRSS2

d $log_2FC = 0.41, p = 1e-62$

TMPRSS2 — T2 Low, T2 High

e $r = -0.61, p = 3e-72$

T2 mucus secretory Network eigengene vs ACE2

f $r = -0.7, p = 2e-102$

Canonical T2 biomarker Network eigengene vs ACE2

g $log_2FC = -0.53, p = 2e-48$

ACE2 — T2 Low, T2 High

a ALI d1 — Expansion(48h)

Mucociliary differentiation

Acute IL-13 (72h) — Chronic IL-13 (10d) — Harvest

b ACE2

FDR = 4.8e-3
log$_2$FC = -0.672

Norm. expression

CTRL   IL-13

c TMPRSS2

FDR = 5.17e-9
log$_2$FC=1.195

Norm. expression

CTRL   IL-13

d

- Prolif. basal
- Diff. basal 1
- Diff. basal 2
- Early sec.
- Intermediate sec.
- Mucus sec.
- IL-13 mucus sec.
- IL-13 inflammatory
- Rare cells
- Early cil. (ctrl only)
- Ciliated

e ACE2

Norm. expression

Control   IL-13

Prolif. basal, Diff. basal 1, Diff. basal 2 *, Early sec., Intermediate sec. *, Mucus sec., IL-13 mucus sec., IL-13 inflammatory, Rare cells, Early cil. (ctrl only), Ciliated

f TMPRSS2

Norm. expression

Control   IL-13

Prolif. basal *, Diff. basal 1 *, Diff. basal 2, Early sec. *, Intermediate sec. *, Mucus sec. *, IL-13 mucus sec. *, IL-13 inflammatory *, Rare cells, Early cil. (ctrl only), Ciliated

a $r = 0.74, p = 2.55e\text{-}120$

b $r = 0.72, p = 1.52e\text{-}110$

c

Network (color)	Network size (# genes)	Hub genes	Pathway enrichment	Cell-type enrichment
Cytotoxic immune response (purple)	417	IKZF3 CD3E CXCR3 CCR5 NKG7	T cell receptor signaling pathway (*p-adj: 6e-16*)	CD8 effector T (*p-adj: 5e-45*)
			Antigen processing and presentation of peptide antigen via MHC class II (*p-adj: 1e-7*)	Dendritic cell (*p-adj: 5e-22*)
Interferon response (tan)	296	IFIT2 IFIT3 OAS2 MX1 IRF1	Type I interferon signaling pathway (*p-adj: 1e-34*)	Monocyte (*p-adj: 6e-10*)
			AIM2 inflammasome complex (*p-adj: 0.05*)	Macrophage (*p-adj: 1e-8*)

d $p = 3.52e\text{-}34$ $log_2FC = 0.8$

e
- Adenovirus (1)
- Coronavirus (18)
- Coronavirus, Influenza (1)
- Enterovirus (4)
- Influenza (20)
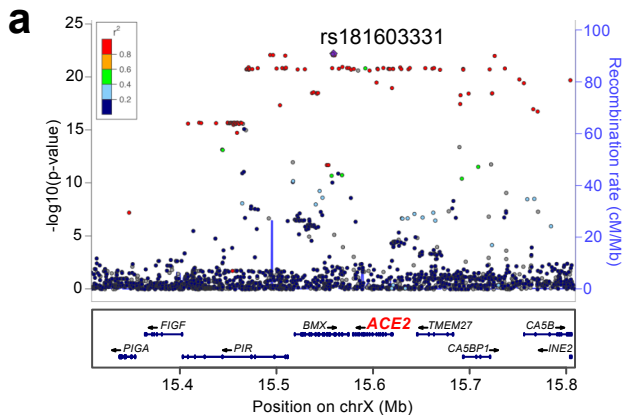- Metapneumovirus (1)
- Parainfluenza (3)
- Rhinovirus (67)
- Rhinovirus, Enterovirus (4)
- RSV (5)

f Expansion (48h)

Differentiation (26 days)

HRV-A16 (24h)

Harvest

g $FDR = 1.29e\text{-}51$ $log_2FC = 2.9$

h $FDR = 0.164$ $log_2FC = -0.4$

a

ΔE_g: 0.059   0.063
p-value: 1.0e-06   3.3e-03

Interferon response network eigengene

Uninfected   HRV⁺   CoV⁺

b

ΔE_g: 0.032   0.049
p-value: 3.7e-05   7.5e-04

Cytotoxic immune response network eigengene

Uninfected   HRV⁺   CoV⁺

c

cellular response to type I interferon:
e.g. *IFITM1, IFI6, IFIT1*
inflammatory response:
e.g. *CXCL11, IL18RAP, TNFRSF8*

CoV⁺   HRV⁺

877   1638   719

cilium movement
e.g. *DNAH1, CFAP61, LRRC6*
axoneme assembly
e.g. *SPAG16, CFAP74, RSPH4A*

d

Upstream Regulator	CoV		HRV	
	Activation Z-score	Enrichment p-value	Activation Z-score	Enrichment p-value
IFNG	11.73	4.04e-110	11.84	9.27e-141
IFNA2	9.04	1.51e-75	8.52	1.40e-74
STAT1	7.88	6.20e-69	7.84	9.33e-83
IFNL1	7.55	2.25e-66	7.28	1.55e-59
TNF	10.16	4.48e-60	11.88	1.74e-98
IRF7	7.89	2.62e-54	8.01	2.40e-57
STAT3	5.00	1.81e-49	6.15	1.72e-77
IL10	2.19	5.44e-49	1.00	1.34e-71
IL1B	8.95	1.64e-47	10.39	4.41e-79
IL6	5.86	1.76e-28	7.32	1.20e-42

e

Top upregulated genes

Shared   CoV⁺ specific   HRV⁺ specific   ACE2 IL6   Cytotoxic pathway genes

iCOS-iCOSL Signaling in T Helper Cells
OX40 Signaling Pathway
Natural Killer Cell Signaling
Cytotoxic T Lymphocyte-mediated Apoptosis of Target Cells
CTLA4 Signaling in Cytotoxic T Lymphocytes

logFC

Cytotoxic pathways
Network
CoV⁺
HRV⁺

f

CoV⁺
NDC80
IL18R1
CD244
BTN3A3
GSDMB
BTN3A1
KIF21B
MAP4K1
JCHAIN
CD8B

Enrichment Score

Up in CD8+ T-cells   Down in CD8+ T-cells

g

Shared   CoV⁺
TBX21   LAT
TXK   BTN3A1
IL32   JCHAIN
CD7   GSDMB
LCK   ACAP1
GZMM   FYN
GZMB   KIF21B
XCL1   PPP1R16B
CD247
GZMH   CD244

Shared
CoV⁺ specific
HRV⁺ specific

Enrichment Score

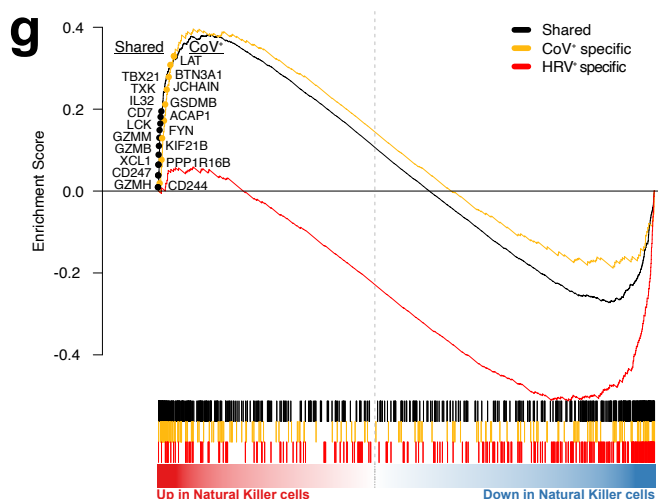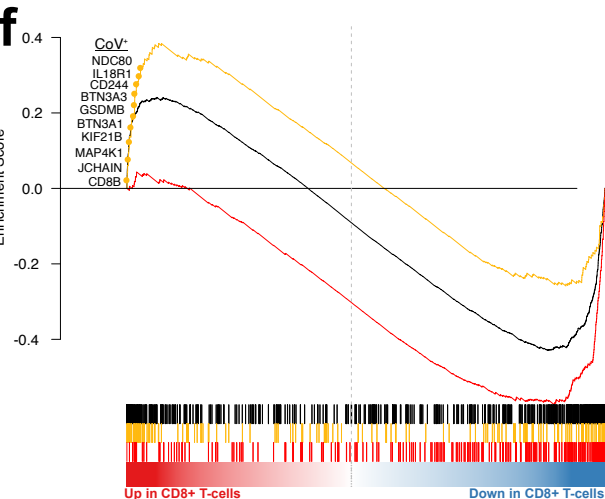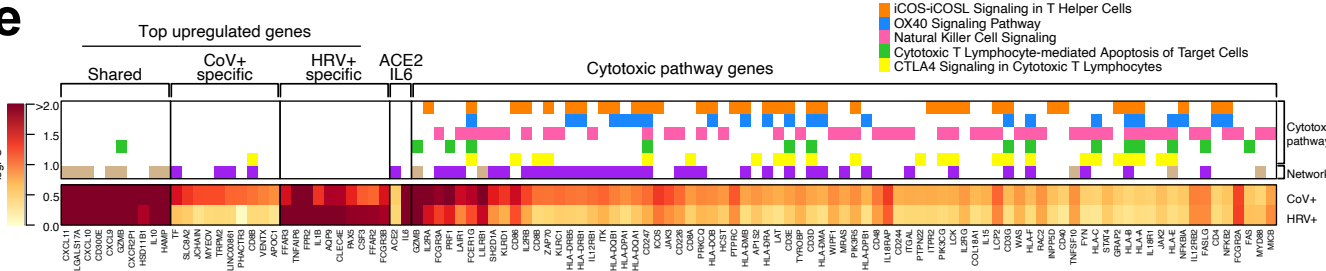Up in Natural Killer cells   Down in Natural Killer cells

Table 1. Results for multivariate models predicting ACE2 and TMPRSS2 expression

Model	Predictor		Partial R^2 (%)	Effect Size		t-test	
	Variable	Ref.		Coeff.	SE	t	p-value
ACE2	Age	*n/a*	1.03	-0.032	0.009	-3.64	0.000300
	Interferon Status	Low	17.09	1.301	0.088	14.78	6.50e-43
	Type 2 Inflammation	Low	24.44	-1.001	0.057	-17.68	1.58e-57
	Sex	Male	0.14	0.075	0.056	1.33	0.185421
	Asthma	Healthy	0.58	-0.160	0.059	-2.73	0.006415
	rs181603331 (G>T)	G/G	1.20	-0.635	0.162	-3.92	0.000097
TMPRSS2	Age	*n/a*	0.07	-0.008	0.010	-0.88	0.380112
	Interferon Status	Low	0.07	0.087	0.098	0.88	0.378731
	Type 2 Inflammation	Low	33.24	1.177	0.063	18.77	1.74e-63
	Sex	Male	0.02	-0.031	0.062	-0.50	0.616276
	Asthma	Healthy	<0.01	0.014	0.065	0.22	0.829301
	rs1475908 (G>A)	G/G	0.22	-0.082	0.054	-1.51	0.130251
	rs74659079 (C>T)	C/C	0.39	0.216	0.107	2.03	0.043151
	rs2838057 (A>C)	A/A	0.42	0.139	0.066	2.12	0.034678